

High-Efficiency CRISPR/Cas9 Mutagenesis of the *white* Gene in the Milkweed Bug *Oncopeltus fasciatus*

Katie Reding and Leslie Pick¹

Department of Entomology, University of Maryland, College Park, Maryland 20742

ORCID IDs: 0000-0003-2067-4232 (K.R.); 0000-0002-4505-5107 (L.P.)

ABSTRACT In this manuscript, we report that clustered regularly interspaced short palindromic repeats (CRISPR)/Cas9 is highly efficient in the hemipteran *Oncopeltus fasciatus*. The *white* gene is well characterized in *Drosophila* where mutation causes loss of eye pigmentation; *white* is a reliable marker for transgenesis and other genetic manipulations. Accordingly, *white* has been targeted in a number of nonmodel insects to establish tools for genetic studies. Here, we generated mutations in the *Of-white* (*Of-w*) locus using CRISPR/Cas9. We found that *Of-w* is required for pigmentation throughout the body of *Oncopeltus*, not just the ommatidia. High rates of somatic mosaicism were observed in the injected generation, reflecting biallelic mutations, and a high rate of germline mutation was evidenced by the large proportion of heterozygous G1s. However, *Of-w* mutations are homozygous lethal; G2 homozygotes lacked pigment dispersion throughout the body and did not hatch, precluding the establishment of a stable mutant line. Embryonic and parental RNA interference (RNAi) were subsequently performed to rule out off-target mutations producing the observed phenotype and to evaluate the efficacy of RNAi in ablating gene function compared to a loss-of-function mutation. RNAi knockdowns phenocopied *Of-w* homozygotes, with an unusual accumulation of orange granules observed in unhatched embryos. This is, to our knowledge, the first CRISPR/Cas9-targeted mutation generated in *Oncopeltus*. While we were unable to establish *white* as a useful visible marker for *Oncopeltus*, these findings are instructive for the selection of visible markers in nonmodel species and reveal an unusual role for an ortholog of a classic *Drosophila* gene.

KEYWORDS *Oncopeltus*; CRISPR; pigmentation; *white*; Hemiptera; emerging model organism

RESearchers using the classic insect model *Drosophila melanogaster* rely on genetic tools and techniques that have accumulated and been refined in this system for over a century. In nonmodel systems, clustered regularly interspaced short palindromic repeats (CRISPR)/Cas9-targeted mutagenesis provides a way to generate both somatic and germline mutations, allowing researchers working with such systems to begin to “catch up” and pursue functional genetic analyses. Visible markers are key tools for such analyses, as they allow mutant or transgenic lines to be perpetuated in the laboratory without the need for molecular analysis (such as PCR) to monitor genotypes at every generation.

Drosophila white is one of the most historically significant genes and remains a useful visible marker for *Drosophila* stocks to this day, over 100 years after its discovery [reviewed in Bellen and Yamamoto (2015)]. At its genesis, Thomas Hunt Morgan’s *white* mutant—lacking eye pigment and thus displaying white rather than red eyes—revealed the phenomenon of sex-linked inheritance (Morgan 1910). The utility of visible markers in both classical genetics and modern molecular genetics cannot be overstated. For example, calculations of recombination frequencies between various visible markers enabled the first known *Drosophila* genes to be mapped. Much later, instability of the *white* phenotype in M cytotype flies helped elucidate the mechanism behind P-M hybrid dysgenesis (Bingham *et al.* 1982). Shortly thereafter, the first *Drosophila* transgene successfully rescued the *rosy* eye color phenotype (Rubin and Spradling 1982). Today, balancer chromosomes with dominant visible markers allow the easy preservation of homozygous lethal alleles. Transgenesis routinely employs *white* as a scorable visible marker (Klemenz *et al.* 1987) and sophisticated genetic tools label somatic clones with

Copyright © 2020 by the Genetics Society of America

doi: <https://doi.org/10.1534/genetics.120.303269>

Manuscript received April 16, 2020; accepted for publication May 21, 2020; published Early Online June 2, 2020.

Available freely online through the author-supported open access option.

Supplemental material available at figshare: <https://doi.org/10.25386/genetics.12339332>.

¹Corresponding author: Department of Entomology, University of Maryland, 4291 Fieldhouse Drive, College Park, MD 20742. E-mail: lpick@umd.edu

fluorescent markers. While it is not realistic to try to replicate all of these genetic tools in other insect species, it is certainly possible to replicate some of them. As more and more researchers broaden their analyses to other insect clades, delving into the unique adaptations within particular groups and the divergence between groups, the development of basic genetic tools in other insects is clearly needed.

Oncopeltus fasciatus, a hemipteran insect in the family Lygaeidae, was once a widely used model species, central to basic studies of insect biochemistry, development, and reproduction [reviewed in Chipman (2017)]. Before the acceleration of *Drosophila* genetics in the early 1980s, several *Oncopeltus* mutant lines had been isolated after treatment with the mutagen ethyl methanesulfonate. In 1970, Peter Lawrence described two new pigmentation mutant lines: one with red eyes (*red eye*, *re*), and another with brown eyes and a white body (*white body*, *wb*) (Lawrence 1970). However, as the era of *Drosophila* genetics advanced and *Oncopeltus* lost favor, these lines and others were apparently lost (Liu and Kaufman 2009; Chipman 2017). More recently, *Oncopeltus* has regained its earlier prominence, as researchers interested in evolutionary developmental biology, aposematism, epigenomics, and toxicology (Panfilio *et al.* 2006; Liu *et al.* 2014; Lohr *et al.* 2017; Auman and Chipman 2018; Bewick *et al.* 2019; Reding *et al.* 2019) have once again turned to the milkweed bug, profiting from its ease of care and high fecundity. Consequently, the value of *Oncopeltus* lines with visible mutations has increased anew.

Here, we provide evidence for the high efficiency of CRISPR/Cas9 mutagenesis in *Oncopeltus* by targeting *white* (*w*), a gene known to be required for proper transport of pigment precursors in the eyes of many insects (Grubbs *et al.* 2015; Li *et al.* 2018; Ohde *et al.* 2018; Xue *et al.* 2018). This gene was chosen to evaluate the utility of the CRISPR/Cas9 genome editing system in this species as it was expected to produce an easily observed phenotype in homozygotes. In addition, a white-eyed *Oncopeltus* line would greatly benefit the field, providing a marker of transgenesis when rescued, allowing easy visualization of fluorescent proteins expressed in the eyes (Berghammer *et al.* 1999), and reducing the effort of screening for homology-directed repair events (Kane *et al.* 2016). Our studies demonstrate the high efficiency of mutagenesis at the *Of-white* locus, using several different guide RNAs (gRNAs) co-injected with Cas9 protein. Biallelic hits were observed in injected G0 hatchlings, resulting in translucent patches throughout the entire body. Surprisingly, no viable *Of-w^{-/-}* homozygotes were obtained, suggesting that this locus is required for viability in *Oncopeltus*.

Materials and Methods

Phylogenetic analysis

The *D. melanogaster* White amino acid sequence was used as the query for a Basic Local Alignment Search Tool (BLAST)-Like Alignment Tool (BLAT) search of the *Oncopeltus* genome

(Panfilio *et al.* 2019). Reciprocal BLAST with the top match suggested the sequence on scaffold 381 was likely the *Oncopeltus* ortholog of *white*. However, since several closely related ABC transporters in the G subfamily have well-characterized roles in pigment transport in insects, we subjected this sequence to a more rigorous test of orthology by performing a phylogenetic analysis. Theoretical translations of the *Drosophila white*, *brown*, and *scarlet* genes were used as queries in searches of the *Oncopeltus* genome. All search results with significance values in the order of $1e-5$ or less were considered, yielding five candidate sequences. Similar searches in the *Halyomorpha halys* genome (Sparks *et al.* 2020) were also performed to gather additional hemipteran sequences; in some cases these sequences were used to better assemble the orthologous *Oncopeltus* gene. tBLASTn searches of the nr/nt database were performed with *Drosophila* sequences as queries to find additional insect sequences. Since *white*, *scarlet*, and *brown* are part of the ABCG subfamily, often one of the largest ABC transporter subfamilies in arthropod genomes (Dermauw and Van Leeuwen 2014), our candidate sequences may include ABCG genes unrelated to pigmentation. To account for this, we added the full set of ABCG genes identified by Broehan *et al.* (2013), with the addition of *brown*, which was identified in a later study (Grubbs *et al.* 2015), to our analysis.

A multiple sequence alignment was generated using Multiple Sequence Comparison by Log-Expectation (MUSCLE). Sequences from the ABCH subfamily were included as an outgroup. The final multiple sequence alignment (Supplemental Material, File S1) was trimmed in AliView and imported into Topali v2.5. Phylogenetic analysis was run using Bayesian inference (MrBayes) with the Jones-Taylor-Thornton (JTT) substitution model and γ -distributed rate model. The tree was then outgroup-rooted and formatted in FigTree v1.4.4 (Figure 1 and File S2).

gRNA design and injection mix

gRNAs were designed using CHOPCHOP (Labun *et al.* 2019) with *Of-w* exon 2 as the target sequence, which yielded 30 candidate gRNA sequences. All 30 sequences were searched in the *O. fasciatus* genome (Panfilio *et al.* 2019) using BLASTn optimized for short queries with the blastn-short option. All resulting alignments were evaluated for the number of exact matches to the protospacer-adjacent motif (PAM) plus the seed sequence (10–12 PAM-proximal nucleotides; Cong *et al.* 2013) to estimate the number of off-target matches. Three gRNA sequences predicted to have zero off-target matches were selected, named gRNAs A, B, and C (Figure 2A). gRNAs A and B have a guanine in the PAM-proximal position, while gRNA C does not; a guanine in this position has been shown to correlate with gRNA efficiency (Doench *et al.* 2014). DNA oligos were designed using these target sequences, with the T7 RNA polymerase promoter sequence added to the 5' end and a primer for the gRNA scaffold sequence added to the 3' end (*Of-w*-exon2-guideA, *Of-w*-exon2-guideB, and *Of-w*-exon2-guideC, see

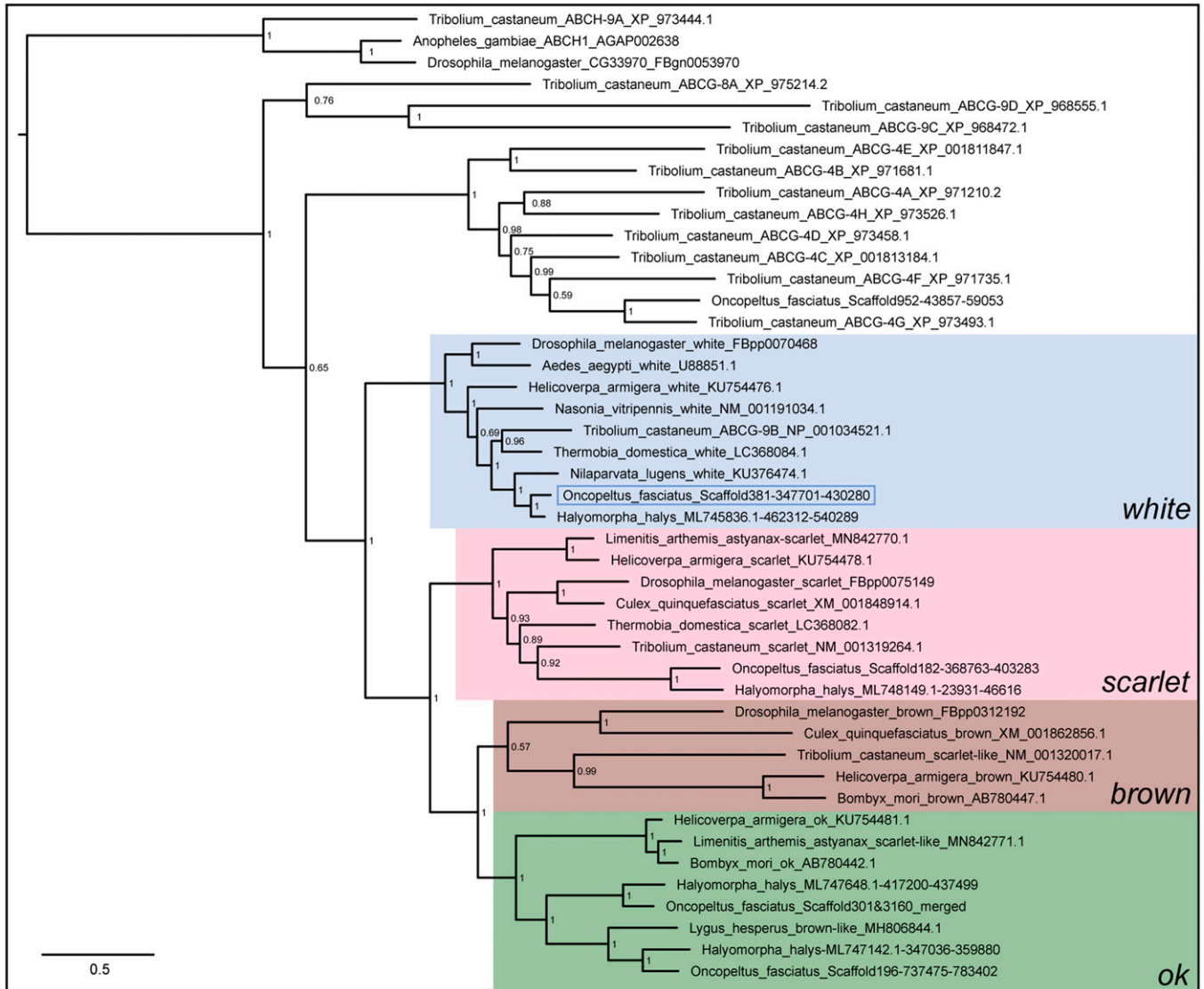


Figure 1 Phylogenetic analysis of ABC transporter subfamily G identifies the *Of-w* ortholog. A gene tree showing relationships between ABC transporter subfamily G members—including *white*, *scarlet*, *brown*, and *ok*—individually highlighted for clarity. The sequence found on scaffold 381 of the *Oncopeltus* genome falls within the *white* clade (blue box). Interestingly, searches of both the *Oncopeltus* and *Halyomorpha* genomes did not reveal clear *brown* orthologs, though two orthologs of *ok* were identified in each. ABC transporter subfamily H genes were included as an outgroup and used to root the tree. Numbers at nodes report posterior probabilities.

Table S1 for sequences). These primers were each used with a common reverse primer (gRNAREV, see Table S1) to amplify the gRNA scaffold sequence from the pCFD3-dU6:3gRNA plasmid (Port *et al.* 2014). PCR products were then purified using the Monarch PCR cleanup kit (New England Biolabs, Beverly, MA). gRNAs were then *in vitro* synthesized using the Megascript T7 kit (Invitrogen, Carlsbad, CA), treated with TURBO DNase (Invitrogen), and purified using the Monarch RNA cleanup kit (New England Biolabs).

Each gRNA was then diluted in injection buffer (5 mM KCl and 0.1 mM phosphate buffer pH 6.8), denatured at 70° for 2 min, transferred to ice for 1 min, then complexed with Cas9-NLS (nuclear localization sequence) protein (PNA Bio) by incubation at room temperature for 5 min. The final concentrations of gRNA and Cas9 protein in the injection mix

were 80 and 300 ng/μl, respectively, as used by others (Kistler *et al.* 2015). The injection mix was centrifuged at 13,000 rpm at 4° for 10 min prior to injection.

RNA interference

The *Of-w* template for double-stranded RNA (dsRNA) was made by PCR-amplifying a 519-bp fragment of *Of-w* from 0 to 120 hr after egg laying (AEL) embryonic complementary DNA (cDNA) using primers *Of-w*-RNAi-FT7 and *Of-w*-RNAi-RT7, which both have the T7 RNA polymerase promoter sequence at the 5' end (see Table S1). This region spans exons 9–12 (Figure 2Ai, orange bar) and therefore does not overlap the target of CRISPR/Cas9 mutagenesis (exon 2). Furthermore, a BLASTn search of the *Oncopeltus* genome using this dsRNA template sequence as query matched only *Of-w*,

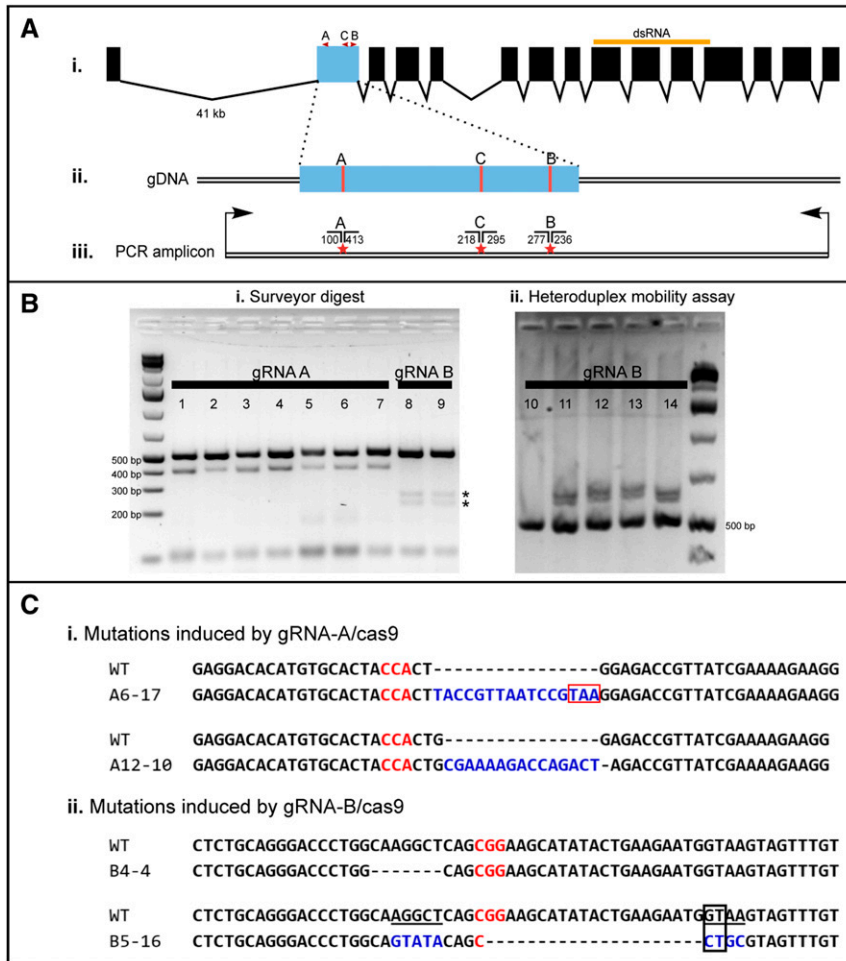


Figure 2 *Oncopeltus* CRISPR/Cas9 mutagenesis workflow. (A) (i) Genomic structure of *Of-w*; exon boundaries are based on transcriptome data and the alignment of a cDNA sequenced in this study to the genome; however, exon 4 was not found in the genome. The dsRNA target region (519 bp) used in this study is shown as an orange bar (exons only). (ii) The target location gRNAs (A–C) used in this study are in red. (iii) The primers used to PCR-amplify exon 2 for our two genotyping assays are shown as black arrows. The amplicon is 513 bp and includes some intronic regions surrounding the exon. Stars mark the predicted loci of Cas9 cleavage and thus likely mutation; the predicted Surveyor cleavage product sizes (in base pairs) for each gRNA are shown above the strands. (B) Gels showing representative results from the Surveyor digest and the heteroduplex mobility assays used to genotype G1s. (i) In the Surveyor assay, PCR products were digested with Surveyor nuclease, resulting in cleavage in samples derived from heterozygous individuals. All gRNA A individuals screened here (lanes 1–7) show the expected cleavage products (~100 and 413 bp), as do all gRNA B individuals (lanes 8–9; ~277 and 236 bp, asterisks), identifying all individuals shown here as heterozygotes. (ii) In the heteroduplex mobility assay, 5 μ l of PCR product was electrophoresed on a 4% agarose gel for > 5 hr at 80 V, allowing visualization of heteroduplexes, which migrate more slowly than homoduplexes, in samples from heterozygotes (lanes 11–14); thus, samples from homozygous individuals (WT) should produce only the 513-bp band (lane 10). (C) Sequenced mutant alleles induced by (i) gRNA-A/Cas9 and (ii) gRNA-B/Cas9. Red and blue lettering indicate the PAM site and insertions, respectively. (i) The mutant allele from individual A6-17 has a 16-bp

insertion (blue) that adds a premature stop codon (red box); the allele from individual A12-10 has a 15-bp insertion (blue) and 1-bp deletion that induces a frameshift. (ii) The allele from individual B4-4 has a 7-bp deletion, resulting in a frameshift; the allele from individual B5-16 is complex, showing substitutions (blue) replacing sequence (underlined) 5' and 3' of the PAM site (red), including mutation of the splicing donor site (black box). cDNA, complementary DNA; CRISPR, clustered regularly interspaced short palindromic repeats; dsRNA, double-stranded RNA; gRNA, guide RNA; PAM, protospacer-adjacent motif; WT, wild-type.

suggesting that it should induce a specific knockdown of *Of-w*. The Megascript T7 kit (Invitrogen) was used to transcribe RNA, which was then DNase-treated, denatured by heating to 94° for 3 min, and reannealed by slowly cooling to 45° over 1 hr. The dsRNA was then precipitated with ethanol and 7.5 M LiCl, spun down, and resuspended in water. The concentration of the dsRNA was approximated by using the single-stranded RNA (ssRNA) setting on a Nanodrop Lite. Molarities were estimated using the ssRNA setting of the NEBioCalculator and halving the estimation. For embryonic RNA interference (eRNAi), *Of-w* dsRNA was diluted in injection buffer to 500 ng/ μ l or ~1.5 μ M, and *gfp* dsRNA was diluted to 650 ng/ μ l or ~1.5 μ M. Embryo injections were carried out as described below. As hatch rate after embryonic injection can vary greatly between replicates due to variation in needle size, embryos that clearly died from injection were excluded from our calculations. For parental RNAi (pRNAi), *Of-w* dsRNA was diluted in injection buffer to 2 μ g/ μ l or ~6 μ M, and *gfp* dsRNA was diluted to 2.6 μ g/ μ l or ~6 μ M. Young adult females were injected using glass

needles between the fourth and fifth abdominal sternites with 5 μ l of the dsRNA dilution. Each injected female was paired with one male; pairs were maintained at 25° and embryos were collected daily from each pair.

Embryonic injection

To collect embryos for injection, cotton was placed in cages with adult *Oncopeltus*, and the bugs were allowed to lay for 5 hr. Embryos were then removed from the cotton, placed in *Drosophila* embryo collection baskets, and washed with water to remove cotton fibers and other debris. To fix the embryos to a surface for injection, several approaches were tested. We found that *Oncopeltus* embryos will not stick to double-sided tape and that various glues encase the embryos in a hard shell from which hatchlings cannot escape. Instead, we designed and three-dimensionally-printed a mold (Figure S1, A and B, and Files S3 and S4) using acrylonitrile butadiene styrene (ABS) filament similar to those designed by others (Porazinski *et al.* 2010; Ohde *et al.* 2018). When filled with molten 3% *Drosophila* food-grade agarose and allowed

to harden, these molds produced 38 × 50-mm agar sheets with grooves roughly equal in width (~0.5 mm) to that of an *Oncopeltus* embryo (Figure S1C). Embryos were lined up longitudinally within the grooves of these agar sheets (Figure S1, D and E), roughly 100 embryos per sheet.

Embryos were injected at 2–8 hr AEL. Needles for injection were pulled from borosilicate glass capillaries (1.0 mm outside diameter, 0.75 mm inner diameter; World Precision Instruments) on a Sutter P-97 needle puller using the following settings: Heat 535, Pull 90, Velocity 100, and Time 160. Needles were opened by clipping the end with fine dissection scissors so that the tip remained flexible. Needles were back-loaded with the injection mix, attached to a Narishige IM-400 microinjector and micromanipulator. The microinjector was programmed for ~6–9 Psi injection pressure and 0.05 sec injection time, and embryos were injected at the posterolateral side. Each sheet of injected embryos was then placed in a sterile petri dish and allowed to develop at 25°. We found that the fungus that grew readily on the agar sheets could be combated by brushing it daily with 70% ethanol using a fine paintbrush. Hatched G0 individuals were transferred to *Drosophila* vials with a strip of seed paper, made by fixing raw organic sunflower seeds to paper with nontoxic wallpaper paste. A constant source of water was supplied by filling the vial one-quarter of the way with water, then inserting a cotton-ball plug to wick water from the bottom of the vial as it dried out. We kept the vials horizontal to reduce the chance of debris coming into contact with the wet cotton, which promotes fungal growth. Once vials became dirty, bugs were CO₂-anesthetized and transferred to clean vials.

Crossing scheme

All 20 CRISPR/Cas9-injected G0s that reached adulthood were mated to wild-type individuals. For these crosses, a single male or female G0 was crossed to one wild-type female or male, respectively, in *Drosophila* vials, as described above, with the addition of a small piece of cotton provided as an egg-laying substrate. Embryos were collected from each pair and G1 individuals were moved to their own vial upon hatching. G1 progeny were reared to adulthood, at which point several individuals from each G0 cross were genotyped by removal of one mesothoracic leg (see below, Figure S2). Each line was self-crossed (e.g., A4 × A4) and also outcrossed to another gRNA-derived line (e.g., A4 × B5), and in most cases crossed to a different line derived from the same gRNA (e.g., A4 × A2). In many cases, these crosses were repeated more than once to increase the likelihood that progeny would be obtained from each combination. As there were more G1 adults than could be reasonably genotyped, many additional crosses were set up “blindly” between individuals of unknown genotypes for a total of 196 G1 crosses.

Screening G1s for heterozygosity

At the last nymphal instar or after molting to adulthood, one mesothoracic leg was removed, placed in a 0.2-ml tube, and crushed with a pipette tip. Next, 50 μl of DNA extraction

buffer (10 mM Tris-HCl pH 8.2, 1 mM EDTA, 25 mM NaCl, and 0.2 mg/ml proteinase K) were added to each tube. Tubes were then incubated for 30 min at 37°, followed by 2 min at 95° to inactivate the proteinase K. *Of-w* exon 2 was then amplified by PCR from the extracted gDNA with primers *Of-w*-exon2-64-F and *Of-w*-exon2-211-R (see Table S1) using Phusion polymerase, yielding a 513-bp product that included some of the flanking introns (Figure 2A).

To determine the genotype of G1s (homozygous wild-type or heterozygous), the *Of-w* exon 2 PCR products were then subjected to one of two assays: the Surveyor nuclease assay or a heteroduplex mobility assay. The Surveyor mutation detection kit (Integrated DNA Technologies) was used for the nuclease assay following the manufacturer's instructions, with the exception that only 1 μl of Surveyor nuclease, rather than the suggested 2 μl, was used. The nuclease reaction products were then run on a 2% gel; the expected cleavage products for offspring of G0s injected with gRNA A are 100 and 413 bp, and those for gRNA B are 277 and 236 bp (Figure 2Bi). The heteroduplex mobility assay was performed following the recommendations of Bhattacharya and Van Meir (2019). Briefly, 5 μl of each PCR product were run on a 4% agarose gel at 80 V for > 5 hr. As heteroduplexes formed by copies of the mutant allele annealing to copies of the wild-type allele migrate more slowly through the agarose matrix than homoduplexes, heterozygotes can be identified by the presence of an extra band when PCR products are run on highly concentrated agarose gels (Figure 2Bii).

For four G1s (Figure 2C), the *w* exon 2 Phusion PCR product was A-tailed by incubation of the purified product with Taq polymerase, TA-cloned into the pGEM-T Easy vector (Promega, Madison, WI), and Sanger-sequenced (Genewiz).

Data availability

All reagents generated in this study are available upon request. File S1 contains the multiple sequence alignment used for phylogenetic analysis. File S2 contains the Newick-formatted tree estimation. Files S3 and S4 are stereolithographic (STL) files of the agar mold design. The authors affirm that all data necessary for confirming the conclusions of the article are present within the article, figures, and tables. Supplemental material available at figshare: <https://doi.org/10.25386/genetics.12339332>.

Results

Gene isolation and experimental design

After subjecting several candidate *white* sequences from the *Oncopeltus* genome to phylogenetic analysis (see *Materials and Methods* for details), only one candidate gene was found to clearly fall within the clade of insect *white* genes, indicating that this sequence is likely the only ortholog of *white* in *Oncopeltus* (Figure 1). This sequence, found on scaffold 381, is nested within the hemipteran *white* clade, and we therefore designate this sequence *Of-white*.

Genome sequence was used to design primers to verify most of the *Of-w* cDNA sequence (*Of-w*-exon1-UTR-F and *Of-w*-R-1, Table S1), from exons 1 to 14. A single, 1.93-kb fragment was isolated from 0 to 120-hr AEL embryonic cDNA. This fragment was sequenced and exon boundaries were determined by alignment to the genome, and validated by the available nymphal and adult transcriptome data (Panfilio *et al.* 2019); this sequence has been deposited at GenBank with accession number MT439905. The cDNA includes an exon 4 (139 bp) that is not found in the genome, but is homologous to the corresponding region in other insect *white* genes. We also found that exon 5 is misplaced in the genome assembly, mapping 5' to exon 2. Given these discrepancies, we also aligned the *Of-w* sequence to the *Halyomorpha white* sequence and verified that the predicted exon boundaries matched nearly identically. *Of-w* has 15 exons spanning a region of ~82.5 kb in the genome assembly (~78 kb in *Halyomorpha*).

To generate loss-of-function mutations in *Of-w*, three different gRNAs—named A, B, and C—were designed to target exon 2 (Figure 2A). We chose to target the beginning of the gene rather than a functional domain, as any frameshift mutations that occur by nonhomologous end joining following the Cas9-induced double-stranded break are more likely to ablate protein function the closer they are to the 5' end.

High rates of somatic mutation were observed in G0 individuals

To generate heritable germline mutations, CRISPR reagents should be injected before cellularization of the embryo as close to the primordia of the germline nuclei as possible. While a precise range of time over which cellularization of the syncytial blastoderm occurs in *Oncopeltus* has not been definitively reported, a cellular blastoderm has been observed by 17 hr AEL at 21° (Butt 1949) and 20 hr AEL at 28° (Ewen-Campen *et al.* 2013). We injected 2–8-hr AEL embryos to ensure that cellularization had not yet occurred. It has been shown that germline induction occurs zygotically in *Oncopeltus* near the site of blastopore formation at the posterior end (Ewen-Campen *et al.* 2013); thus embryos were injected laterally near the posterior pole. Embryos were collected over 5 hr and individually injected with one of the three gRNAs complexed with purified Cas9 protein (Figure 2A). G0 individuals injected with gRNAs A or B showed high rates of somatic biallelic mutation upon hatching, evidenced by clear mosaic loss of pigment throughout the body (Figure 3). In some cases, large translucent patches were observed, often delineated by distinct compartment boundaries (e.g., Figure 3, B, C, and I). Mosaic loss of pigment in the compound eyes was most apparent in adults (Figure 3, E–G). Of the G0 individuals that hatched, those that had been injected with gRNA A showed the highest rate of mosaicism (Figure 4, 92.5% of hatchlings, 37/40), followed by those injected with gRNA B (75%, 9/12). Only 14% of bugs injected with gRNA C displayed similar mosaic loss of pigment, and this group showed the highest hatch rate (Figure 4, 83%, 99/119). Since a lower rate of somatic mutation was observed in this group, all

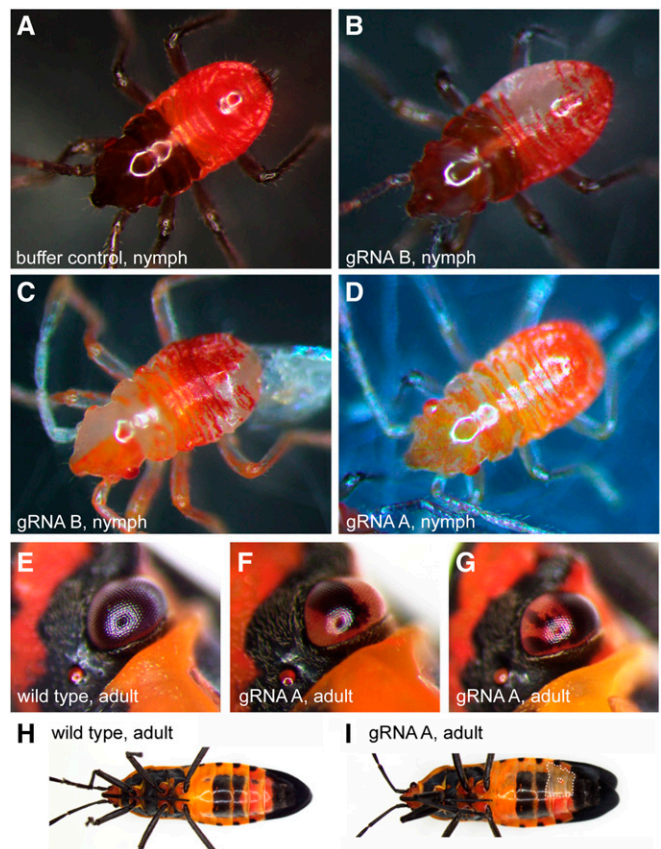


Figure 3 High rates of somatic mutation were observed after *Of-w* CRISPR mutagenesis. Examples of first-instar nymph hatchlings at varying stages (A–D) or adults (E–I) after injection of embryos with buffer or gRNAs and Cas9, are shown. (A) Nymph post-melanization, control injection with buffer; (B) nymph mid-melanization, gRNA-B; large translucent patches can be seen in the abdomen; and (C) nymph pre-melanization, gRNA-B; mosaic translucent patches are obvious in the right half of the head and patches in the thorax, abdomen, and appendages. (D) Nymph pre-melanization, gRNA-A; translucent regions can be seen throughout the body; (E) adult compound eye, wild-type; (F) adult compound eye, gRNA-A, individual A-14; and (G) adult compound eye, gRNA-A, individual A-13. The black pigmentation seen in wild-type is absent from sections of the eye in these two individuals (F and G). (H) Wild-type pigmentation in adult body, ventral view. (I) Mosaic loss of pigmentation in lateral patch (dotted white outline) in adult body, gRNA-A, individual A-13, ventral view. CRISPR, clustered regularly interspaced short palindromic repeats; gRNA, guide RNA.

subsequent observations and analyses were made with gRNA groups A and B only.

Germline transmission of white mutations

In some insects, the ability to singly mate individuals is precluded by various behavioral adaptations favoring swarming and other nonmonogamous mating systems. For a species to be amenable to genetic studies, it is necessary to be able to control copulations by singly mating individuals, which we were able to do for *Oncopeltus* (see *Materials and Methods*). Each injected G0 adult was mated to a wild-type individual by placing the pair in a *Drosophila* vial with a water source and sunflower seeds (see *Materials and Methods* for more

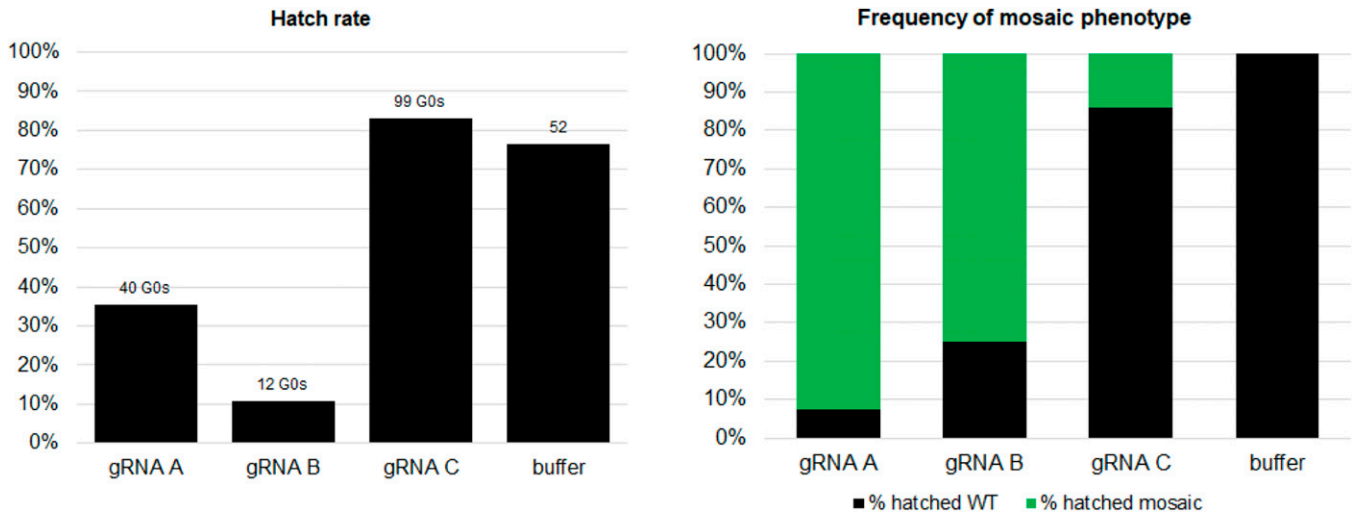


Figure 4 Somatic mosaicism and hatch rate varied after CRISPR/Cas9 embryonic injection with different guide RNAs. (A) Hatch rate of embryos injected with gRNAs (A–C) compared to those injected with buffer. (B) Frequency of mosaic pigmentation phenotype in G0s. Embryos injected with gRNAs A or B clearly showed much higher rates of mosaicism than embryos injected with gRNA-C. CRISPR, clustered regularly interspaced short palindromic repeats; gRNA, guide RNA; WT, wild-type.

detail), and embryos from each pair were collected daily. We observed fairly high mortality in the G1 generation during development from embryo to adult; the cause of death frequently appeared to be an inability to shed the exoskeleton while trying to molt (data not shown). The eye and body pigmentation of all G1s was indistinguishable from wild-type. Adult G1s were obtained from 16 of 20 G0s (11 A lines and 5 B lines). In total, 161 G1s were genotyped using the Surveyor or heteroduplex mobility assays (see *Materials and Methods*) on DNA extracted from a clipped leg, allowing us to mate individuals after genotyping; 104 were genotyped as heterozygous at the *Of-w* locus (64.6%). Only two G0 lines yielded no G1 progeny genotyped heterozygous (Figure S2); one of these G0s (A3) had shown no mosaic loss of pigment, while mosaicism was observed in the other (A11). This high rate of germline mutation may have been biased by the fact that somatic mutations could be visibly observed in the G0s, allowing us to prioritize G1s based on the parental G0 phenotype. Of the 14 G0s that yielded heterozygous progeny, only one of these was not an obvious phenotypic mosaic.

Sequences of *Of-w* exon 2 from four G1 heterozygotes that had given $w^{-/-}$ progeny showed insertion/deletions at the expected double-stranded break site, resulting in frameshifts and subsequent premature stop codons in almost every case, likely leading to nonsense-mediated decay of the transcripts (Figure 2C). The mutation isolated from individual A6-17 has a 16-bp insertion, including insertion of an in-frame premature stop codon (Figure 2Ci, red box). The predicted full-length coding DNA sequence (CDS) of *Of-w* is 2052 bp; the A6-17 allele encodes a stop codon at nucleotide position 132, or 6% wild-type CDS length. The mutant allele isolated from individual A12-10 has a 15-bp insertion coupled with a 1-bp deletion, resulting in a stop codon at 13% wild-type CDS length. The B4-4 mutation has a 7-bp deletion and a stop

codon at 15% wild-type CDS length. The B5-16 has 5- and 4-bp substitutions upstream and downstream of the PAM site, respectively, along with a 21-bp deletion between the two substitutions, which does not result in a frameshift. However, the second substitution disrupts the GT splice donor site.

In sum, while germline mutation was clearly mosaic, we observed high rates of overall germline mutation with 14 of the 16 fertile G0 lines showing transmission of a mutant allele to at least one offspring.

Despite germline transmission, homozygous white hatchlings were not recovered

To establish stable mutant lines, G1 individuals genotyped as heterozygous were crossed to each other. Despite efforts to minimize off-target mutations, these are known to occur after CRISPR mutagenesis even after careful gRNA design (Aryal *et al.* 2018). Indeed, we observed phenotypes such as shortened antennae presumably resulting from off-target mutations over the course of this experiment (data not shown). Therefore, we took advantage of the fact that any mutations present in our G1s were derived from one of two different gRNAs (A or B), allowing us to generate transheterozygous G2s. Assuming that any off-target mutations resulting from gRNA-A/Cas9 would be different from off-target mutations resulting from gRNA-B/Cas9, we set up many A \times B crosses presuming that off-target mutations would be complemented in their progeny.

Given the G0 phenotypes we observed (Figure 3), we expected one-quarter of these G2 offspring to have a white eye and white body phenotype. From many crosses (total of 196), only phenotypically wild-type G2 hatchlings were recovered. As we have observed that first instars will cannibalize unhatched embryos, it seemed likely that if $w^{-/-}$ individuals were developmentally delayed, they would be especially vulnerable to predation by siblings. Therefore,

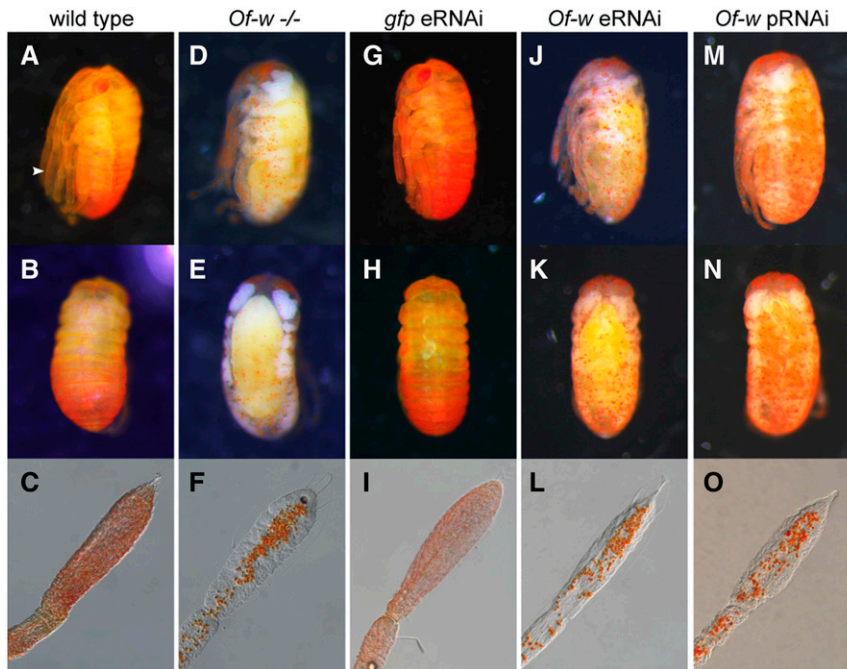


Figure 5 Nonviable *Of-w* homozygotes and RNAi knockdown embryos both display “spotted” phenotype. (A and B) Wild-type phenotype, sibling of embryos shown in (D and E); arrowhead indicates antenna. (C) Last antennal segment of a wild-type individual. (D and E) *Of-w* homozygous mutant phenotype, sibling of embryos in (A and B). (F) Last antennal segment of a $w^{-/-}$ individual. (G–I) *gfp* eRNAi negative control replicates wild-type phenotype. (J–L) *Of-w* eRNAi embryo phenocopies *Of-w* mutant. (M–O) *Of-w* pRNAi embryo phenocopies *Of-w* mutant. (A, D, G, J, and M) Lateral views; (B, E, H, K, and N) dorsal views. (C, F, I, L, and O) Last antennal segment shows clusters of undispersed orange pigment in *Of-w* homozygous mutants (F) and after *Of-w* RNAi (L and O) compared to wild-type dispersion of pigments (C and I). e, embryonic; p, parental; RNAi, RNA interference.

we collected embryos from individual crosses every day to be able to monitor each clutch and remove any hatchlings as quickly as possible. From 21 of these crosses, we observed a similar aberrant pigmentation phenotype in around one-fifth of offspring [mean = $20\% \pm 1.84$ (SE) across $n = 21$ crosses; 1637 embryos examined in total]. These embryos appeared entirely translucent, with the exception of spots of orange pigment throughout the body (Figure 5, D–F), while their wild-type siblings showed normal dispersion of pigment (Figure 5, A–C). This lack of pigment dispersion could best be seen in the antennae (Figure 5, C and F) and other appendages where the orange spots are concentrated in the center. Interestingly, a similar phenotype was not observed in the large $w^{-/-}$ patches seen in some G0 somatic mutants (Figure 3, B and C). Individuals with this “spotted” phenotype were also more fragile when handled compared to their wild-type siblings. This phenotype was observed in progeny of $A \times A$, $B \times B$, and $A \times B$ crosses, suggesting that it is not due to off-target mutations. As soon as this phenotype was visible, usually 2–3 days prior to the expected hatch date, $w^{-/-}$ embryos were separated from their wild-type siblings to ensure they would not be cannibalized; however, none of the $w^{-/-}$ embryos ever hatched. We also observed a subset [mean = $17\% \pm 4.6$ (SE) across $n = 21$ crosses] of the G2 progeny that seemed to lack yolk and appeared flattened; these embryos completely failed to develop. In sum, mutation of *white* is homozygous lethal in *Oncopeltus* and results in a spotted pigmentation phenotype throughout the body.

RNAi produces phenocopies of *Of-w* homozygotes

Given that the lethality observed in the G2 homozygotes was unexpected, we were interested to see if this phenotype could

have been predicted by RNAi and how well parental vs. embryonic RNAi-treated individuals would phenocopy the mutant. Therefore, we injected embryos and adult females with *w* dsRNA (Figure 2A, orange bar) or *gfp* dsRNA as a control. Both eRNAi and pRNAi appeared to phenocopy the $w^{-/-}$ mutant equally well (Figure 5, J–O) compared to *gfp* controls (Figure 5, G–I). The spotted phenotype can be easily seen through the chorion as early as a few days before the expected hatch date (7 days AEL), thus embryos were visually inspected at this time. The presence of eye spots and wild-type dispersion of pigment throughout the body was scored as wild-type, the presence of at least one eye spot and mosaic spotted pigmentation was scored as a partial $w^{-/-}$ phenocopy, and loss of both eyespots and spotted pigmentation throughout the body was scored as a complete $w^{-/-}$ phenocopy. An average of $97\% \pm 0.64$ (SD) of *Of-w* pRNAi offspring ($n = 3$ replicates, 176 embryos examined) phenocopied the *Of-w* homozygotes, compared to 0% of the offspring from the *gfp* dsRNA-injected controls ($n = 4$ replicates, 175 embryos examined). Similarly, $96.7\% \pm 3.1$ (SD) of *w* dsRNA-injected embryos ($n = 2$ replicates, 289 embryos examined) phenocopied the mutant, while an average of $2.3\% \pm 1.7$ (SD) displayed a partial phenocopy, compared to 0% of *gfp* dsRNA-injected control embryos ($n = 2$ replicates, 163 embryos examined).

Discussion

Here, we have shown that CRISPR/Cas9 is highly effective in the milkweed bug *O. fasciatus* and that, unlike many other insect species in which stable *white* mutant lines have been

generated (Morgan 1910; Grubbs *et al.* 2015; Li *et al.* 2018; Ohde *et al.* 2018; Xue *et al.* 2018), *Of-w* mutations are homozygous lethal. Nonetheless, the observed efficiency of this mutagenesis system indicates that creating lines with visible mutations is feasible, once an appropriate candidate gene is identified. This essential role of *white* in *Oncopeltus* viability was not predicted by previous RNAi experiments targeting *Of-w* in *Oncopeltus* nymphs and adults (Liu 2016; A. Popadić, personal communication), emphasizing the importance of testing gene function at every developmental stage by RNAi before proceeding to CRISPR/Cas9 mutagenesis.

While RNAi is known to be effective and has been widely used to knock down gene function in *Oncopeltus*, the *Of-w* mutation reported here is, to our knowledge, the first targeted gene knockout in this species. This allows us to directly compare RNAi knockdown to a loss-of-function genetic mutation. Our results show that both eRNAi and pRNAi replicated the mutant phenotype, suggesting that RNAi is likely sufficient in many cases to produce mutant phenocopies. However, it has also been observed that RNAi phenotypes can be variable, and may depend on the length or amount of the dsRNA injected, the region targeted, or the amount of time since injection (Liu and Kaufman 2004, 2005). In these cases and others in which low protein concentrations may be sufficient for wild-type function, or when a stable mutant line is desirable, CRISPR/Cas9 is an effective alternative strategy.

Due to the lack of definitive “rules” for gRNA design, it is often recommended to test the efficiency of several gRNAs per target to optimize mutagenesis. Our results demonstrate the additional benefit of testing multiple gRNAs, particularly in nonmodel species with fairly long generation times. Of the three gRNAs we tested, all produced mosaic phenotypes; this allowed us to cross lines derived from different gRNAs, producing transheterozygotes whose phenotypes cannot likely be attributed to off-target mutations. If using only one gRNA, off-target mutations can be purged from a line by outcrossing for some number of generations; in species with short generation times, this is a feasible approach. However, even in species with only moderate-length generations like *Oncopeltus*, the ability to observe the mutant phenotypes reasonably quickly (within two generations) is a great advantage.

Despite the high efficiency of mutagenesis in *Oncopeltus*, there are a few challenges specific to this species relative to some other laboratory models. First, *Oncopeltus* take ~6 weeks to mature from embryos to reproductive adults at 25°. Thus, the time between embryo injection to analysis of G2 phenotype was ~120 days at our rearing conditions (~23–26°), though time could be saved by maintaining bugs at slightly higher temperatures. A second challenge that remains for CRISPR/Cas9 mutagenesis in *Oncopeltus* is the frequency of cannibalism among hatchlings. When performing parental RNAi, we have found that at high-enough dsRNA concentrations, all embryos within a single clutch typically share a similar phenotype. For instance, in the case of *Of-w* pRNAi, all embryos within a clutch failed to hatch. However,

when crossing heterozygous mutants, only a fraction of the progeny are expected to display a given phenotype. If this phenotype involves lethality or developmental delay, the homozygous mutant embryos will likely be cannibalized by their nonhomozygous siblings if not kept separate. Separating the homozygous embryos within each clutch once the phenotype becomes visible is time-intensive and may not be possible if the associated phenotype is not visibly apparent.

Lastly, while lethality due to *Of-w* mutation was not expected, it is not wholly unprecedented. Khan *et al.* (2017) showed that in the moth *Helicoverpa armigera*, loss-of-function mutations of *white* are also homozygous lethal. In *Tribolium castaneum*, an RNAi screen of ABC transporters showed that knockdown of another member of the G subfamily (which includes *white*), *Tc-ABCG-4C*, resulted in embryonic mortality and a decrease in lipid transport to the epicuticle and elsewhere in injected larvae (Broehan *et al.* 2013). In the heteropteran *Lygus hesperus* (family: Miridae), knockdown of *white* by RNAi resulted in cuticular and behavioral defects. Yet in another more distantly related hemipteran, *Nilaparvata lugens* (family: Delphacidae), CRISPR/Cas9-induced mutation resulted in viable *white* mutants (Xue *et al.* 2018). It is interesting to note that even in *Drosophila*, mutation of *white* is not without fitness consequences. Xiao *et al.* (2017) showed that *white* is involved in mating success, in a manner independent of its role in eye pigmentation. White-eyed flies with a mutant copy of *white* showed reduced mating success compared to wild-type flies, while white-eyed flies with a wild-type copy of *white* (*w+*; *cn*, *bw*) showed no such decrease.

Although generating a white-eyed *Oncopeltus* strain may not be as simple as mutating one gene, it is certainly possible. Indeed, when mutants heterozygous at the aforementioned *re* and *wb* loci were crossed, the *re*^{-/-}; *wb*^{-/-} offspring had white eyes (Lawrence 1970). Thus, instead of knocking out *white*, which is critical to both the ommochrome and pteridine pathways, the situation in *Oncopeltus* is likely similar to that in *H. armigera*. In this species, a *white* mutation was likewise found to be homozygous lethal (Khan *et al.* 2017). However, white-eyed moths were produced when individuals were homozygous for mutations at the *ok* (*brown* paralog, thus likely part of the pteridine pathway, responsible for the production of red pigments) and *scarlet* (of the ommochrome pathway, responsible for the production of brown pigments) loci. Thus, a potential strategy could be to generate two similar knockouts to disrupt both ommochrome and pteridine pathways in *Oncopeltus* after first investigating gene function by RNAi to rule out lethality or other unexpected phenotypes. The present study shows not only the efficiency of both CRISPR mutagenesis and RNAi in *Oncopeltus*, but also how these techniques complement each other in a nonmodel species. Particularly when gene function cannot be directly inferred from that of homologous genes in other species, these two approaches work well in concert.

Alternatively, one could avoid assumptions of functional conservation altogether; the efficiency of CRISPR/Cas9-induced mutation presented here suggests that homology-directed

repair events may likewise be a viable strategy in this species. Rather than generating loss-of-function mutations, one could insert epitope tags for immunoprecipitation or insert a visible (*i.e.*, fluorescent) tag to a gene of interest. The numerous ways in which visible markers have empowered other genetic model systems affirm the advantage of producing visible mutations. Our studies showed that *Oncopeltus* CRISPR/Cas9 efficiency is often high enough to produce biallelic mutations in injected individuals, greatly aiding selection of individuals and providing immediate evidence of mutation. Thus, testing a number of candidate genes is feasible and could lead to the identification of multiple markers useful in this model system.

Acknowledgments

We thank the teachers and participants of the Insect Genetic Technologies Research Coordination Network (IGTRCN) Technical Workshop: Insect Genetic Technologies: Theory and Practice for their advice with regard to embryo injection and gRNA design; Aleksandar Popadić for his suggestions and for sharing unpublished data; the laboratory of Don Weber for their “seed paper” idea; and Steve Mount and members of the Pick laboratory for their comments on the manuscript. The pCFD3 plasmid (Addgene plasmid number 49410) used to amplify the gRNA scaffold sequence was a gift from Simon Bullock by way of Sougata Roy. This work was supported by a National Institutes of Health grant (R01 GM-113230) to L.P.

Literature Cited

Aryal, N. K., A. R. Wasylishen, and G. Lozano, 2018 CRISPR/Cas9 can mediate high-efficiency off-target mutations in mice *in vivo*. *Cell Death Dis.* 9: 1099. <https://doi.org/10.1038/s41419-018-1146-0>

Auman, T., and A. D. Chipman, 2018 Growth zone segmentation in the milkweed bug *Oncopeltus fasciatus* sheds light on the evolution of insect segmentation. *BMC Evol. Biol.* 18: 178 (erratum: *BMC Evol. Biol.* 163: 772). <https://doi.org/10.1186/s12862-018-1293-z>

Bellen, H. J., and S. Yamamoto, 2015 Morgan’s legacy: fruit flies and the functional annotation of conserved genes. *Cell* 163: 12–14. <https://doi.org/10.1016/j.cell.2015.09.009>

Berghammer, A. J., M. Klingler, and E. A. Wimmer, 1999 A universal marker for transgenic insects. *Nature* 402: 370–371. <https://doi.org/10.1038/46463>

Bewick, A. J., Z. Sanchez, E. C. McKinney, A. J. Moore, P. J. Moore *et al.*, 2019 Dnmt1 is essential for egg production and embryo viability in the large milkweed bug, *Oncopeltus fasciatus*. *Epigenetics Chromatin* 12: 6. <https://doi.org/10.1186/s13072-018-0246-5>

Bhattacharya, D., and E. G. Van Meir, 2019 A simple genotyping method to detect small CRISPR-Cas9 induced indels by agarose gel electrophoresis. *Sci. Rep.* 9: 4437. <https://doi.org/10.1038/s41598-019-39950-4>

Bingham, P. M., M. G. Kidwell, and G. M. Rubin, 1982 The molecular basis of P-M hybrid dysgenesis: the role of the P element, a P-strain-specific transposon family. *Cell* 29: 995–1004. [https://doi.org/10.1016/0092-8674\(82\)90463-9](https://doi.org/10.1016/0092-8674(82)90463-9)

Broehan, G., T. Kroege, M. Lorenzen, and H. Merzendorfer, 2013 Functional analysis of the ATP-binding cassette (ABC) transporter gene family of *Tribolium castaneum*. *BMC Genomics* 14: 6. <https://doi.org/10.1186/1471-2164-14-6>

Butt, F. H., 1949 *Embryology of the Milkweed Bug: Oncopeltus Fasciatus (Hemiptera)*. Cornell University Agricultural Experiment Station, Ithaca, NY.

Chipman, A. D., 2017 *Oncopeltus fasciatus* as an evo-devo research organism. *Genesis* 55: e23020. 10.1002/dvg.23020 <https://doi.org/10.1002/dvg.23020>

Cong, L., F. A. Ran, D. Cox, S. Lin, R. Barretto *et al.*, 2013 Multiplex genome engineering using CRISPR/Cas systems. *Science* 339: 819–823. <https://doi.org/10.1126/science.1231143>

Dermauw, W., and T. Van Leeuwen, 2014 The ABC gene family in arthropods: comparative genomics and role in insecticide transport and resistance. *Insect Biochem. Mol. Biol.* 45: 89–110. <https://doi.org/10.1016/j.ibmb.2013.11.001>

Doench, J. G., E. Hartenian, D. B. Graham, Z. Tothova, M. Hegde *et al.*, 2014 Rational design of highly active sgRNAs for CRISPR-Cas9-mediated gene inactivation. *Nat. Biotechnol.* 32: 1262–1267. <https://doi.org/10.1038/nbt.3026>

Ewen-Campen, B., T. E. M. Jones, and C. G. Extavour, 2013 Evidence against a germ plasm in the milkweed bug *Oncopeltus fasciatus*, a hemimetabolous insect. *Biol. Open* 2: 556–568. <https://doi.org/10.1242/bio.20134390>

Grubbs, N., S. Haas, R. W. Beeman, and M. D. Lorenzen, 2015 The ABCs of eye color in *Tribolium castaneum*: orthologs of the *Drosophila* white, scarlet, and brown genes. *Genetics* 199: 749–759. <https://doi.org/10.1534/genetics.114.173971>

Kane, N. S., M. Vora, K. J. Varre, and R. W. Padgett, 2016 Efficient screening of CRISPR/Cas9-induced events in *Drosophila* using a Co-CRISPR strategy. *G3 (Bethesda)* 7: 87–93. <https://doi.org/10.1534/g3.116.036723>

Khan, S. A., M. Reichelt, and D. G. Heckel, 2017 Functional analysis of the ABCs of eye color in *Helicoverpa armigera* with CRISPR/Cas9-induced mutations. *Sci. Rep.* 7: 40025. <https://doi.org/10.1038/srep40025>

Kistler, K. E., L. B. Vosshall, and B. J. Matthews, 2015 Genome engineering with CRISPR-Cas9 in the mosquito *Aedes aegypti*. *Cell Rep.* 11: 51–60. <https://doi.org/10.1016/j.celrep.2015.03.009>

Klemenz, R., U. Weber, and W. J. Gehring, 1987 The white gene as a marker in a new P-element vector for gene transfer in *Drosophila*. *Nucleic Acids Res.* 15: 3947–3959. <https://doi.org/10.1093/nar/15.10.3947>

Labun, K., T. G. Montague, M. Krause, Y. N. Torres Cleuren, H. Tjeldnes *et al.*, 2019 CHOPCHOP v3: expanding the CRISPR web toolbox beyond genome editing. *Nucleic Acids Res.* 47: W171–W174. <https://doi.org/10.1093/nar/gkz365>

Lawrence, P. A., 1970 Some new mutants of the large milkweed bug *Oncopeltus fasciatus* Dall. *Genet. Res.* 15: 347–350. <https://doi.org/10.1017/S0016672300001713>

Li, M., O. S. Akbari, and B. J. White, 2018 Highly efficient site-specific mutagenesis in malaria mosquitoes using CRISPR. *G3 (Bethesda)* 8: 653–658. <https://doi.org/10.1534/g3.117.1134>

Liu, J., 2016 Unraveling the molecular mechanisms of aposematic pigmentation in *Oncopeltus fasciatus*. Ph.D. Thesis, Wayne State University, Detroit.

Liu, J., T. Lemonds, and A. Popadić, 2014 The genetic control of aposematic black pigmentation in hemimetabolous insects: insights from *Oncopeltus fasciatus*. *Evol. Dev.* 16: 270–277. <https://doi.org/10.1111/ede.12090>

Liu, P., and T. C. Kaufman, 2009 Morphology and husbandry of the large milkweed bug, *Oncopeltus fasciatus*. *Cold Spring Harb. Protoc.* 2009: pdb.emo127. <https://doi.org/10.1101/pdb.emo127>

Liu, P. Z., and T. C. Kaufman, 2004 Hunchback is required for suppression of abdominal identity, and for proper germband

- growth and segmentation in the intermediate germband insect *Oncopeltus fasciatus*. *Development* 131: 1515–1527. <https://doi.org/10.1242/dev.01046>
- Liu, P. Z., and T. C. Kaufman, 2005 even-skipped is not a pair-rule gene but has segmental and gap-like functions in *Oncopeltus fasciatus*, an intermediate germband insect. *Development* 132: 2081–2092. <https://doi.org/10.1242/dev.01807>
- Lohr, J. N., F. Meinzer, S. Dalla, R. Romey-Glusing, and S. Dobler, 2017 The function and evolutionary significance of a triplicated Na,K-ATPase gene in a toxin-specialized insect. *BMC Evol. Biol.* 17: 256. <https://doi.org/10.1186/s12862-017-1097-6>
- Morgan, T. H., 1910 Sex limited inheritance in *Drosophila*. *Science* 32: 120–122. <https://doi.org/10.1126/science.32.812.120>
- Ohde, T., Y. Takehana, T. Shiotsuki, and T. Niimi, 2018 CRISPR/Cas9-based heritable targeted mutagenesis in *Thermobia domestica*: a genetic tool in an apterygote development model of wing evolution. *Arthropod Struct. Dev.* 47: 362–369. <https://doi.org/10.1016/j.asd.2018.06.003>
- Panfilio, K. A., P. Z. Liu, M. Akam, and T. C. Kaufman, 2006 *Oncopeltus fasciatus* zen is essential for serosal tissue function in katatrepsis. *Dev. Biol.* 292: 226–243. <https://doi.org/10.1016/j.ydbio.2005.12.028>
- Panfilio, K. A., I. M. Vargas Jentzsch, J. B. Benoit, D. Erezylmaz, Y. Suzuki *et al.*, 2019 Molecular evolutionary trends and feeding ecology diversification in the Hemiptera, anchored by the milkweed bug genome. *Genome Biol.* 20: 64. <https://doi.org/10.1186/s13059-019-1660-0>
- Porazinski, S. R., H. Wang, and M. Furutani-Seiki, 2010 Microinjection of medaka embryos for use as a model genetic organism. *J. Vis. Exp.* 46: 1937. <https://doi.org/10.3791/1937>
- Port, F., H.-M. Chen, T. Lee, and S. L. Bullock, 2014 Optimized CRISPR/Cas tools for efficient germline and somatic genome engineering in *Drosophila*. *Proc. Natl. Acad. Sci. USA* 111: E2967–E2976. <https://doi.org/10.1073/pnas.1405500111>
- Reding, K., M. Chen, Y. Lu, A. M. Cheattle Jarvela, and L. Pick, 2019 Shifting roles of *Drosophila* pair-rule gene orthologs: segmental expression and function in the milkweed bug *Oncopeltus fasciatus*. *Development* 146: dev181453. <https://doi.org/10.1242/dev.181453>
- Rubin, G. M., and A. C. Spradling, 1982 Genetic transformation of *Drosophila* with transposable element vectors. *Science* 218: 348–353. <https://doi.org/10.1126/science.6289436>
- Sparks, M. E., R. Bansal, J. B. Benoit, M. B. Blackburn, H. Chao, *et al.*, 2020 Brown marmorated stink bug, *Halyomorpha halys* (stål), genome: putative underpinnings of polyphagy, insecticide resistance potential and biology of a top worldwide pest. *BMC Genomics* 21: 227. <https://doi.org/10.1186/s12864-020-6510-7>
- Xiao, C., S. Qiu, and R. M. Robertson, 2017 The white gene controls copulation success in *Drosophila melanogaster*. *Sci. Rep.* 7: 7712. <https://doi.org/10.1038/s41598-017-08155-y>
- Xue, W.-H., N. Xu, X.-B. Yuan, H.-H. Chen, J.-L. Zhang *et al.*, 2018 CRISPR/Cas9-mediated knockout of two eye pigmentation genes in the brown planthopper, *Nilaparvata lugens* (Hemiptera: Delphacidae). *Insect Biochem. Mol. Biol.* 93: 19–26. <https://doi.org/10.1016/j.ibmb.2017.12.003>

Communicating editor: B. Goldstein